Finite-time singularity formation in Hele-Shaw systems

Todd F. Dupont
Computational and Applied Mathematics Program, Ryerson Laboratory, The University of Chicago, Chicago, Illinois 60637

Raymond E. Goldstein
Department of Physics, Princeton University, Princeton, New Jersey 08540

Leo P. Kadanoff
Computational and Applied Mathematics Program, Ryerson Laboratory, The University of Chicago, Chicago, Illinois 60637

Su-Min Zhou
Computational and Applied Mathematics Program, Ryerson Laboratory, The University of Chicago, Chicago, Illinois 60637 and Department of Radiation Oncology, University of California at San Francisco, California 94122

(Received 4 February 1993)

We investigate the behavior of the interface between two fluids in a two-dimensional flow driven by surface tension. The geometry is chosen so that one can apply a variant of the lubrication approximation and so that the more-viscous fluid will have a tendency to change its topology by separating into two masses. Simulations are used to show that, with appropriate initial and boundary conditions, this separation can occur in a finite time. We particularly focus our attention at the pinch point, i.e., the space-time point at which the width of the viscous fluid first goes to zero. The lubrication approximation used contains a parameter ρ which measures the strength of the inertial forces. Since the fluid velocity diverges as the pinch is approached, the behavior is qualitatively different for small ρ and for $\rho=0$. Simulations and asymptotic analyses are used to isolate this difference. For $\rho=0$, at the pinch time there is a region of space in which the width grows quadratically as one moves away from the pinch. The curvatures, however, are different on the two sides of the pinch. In contrast, when ρ is different from zero, the width rises nearly linearly with distance from the pinch.

PACS number(s): 03.40.Gc, 47.20.Ky, 47.15.Hg

I. INTRODUCTION

In a previous paper [1], we described the behavior of a Hele-Shaw [2] cell in the lubrication approximation. Figure 1 shows a Hele-Shaw cell setup. This cell is a quasi-two-dimensional system in which two fluids, which we will simply call air and water, are confined to the narrow space between two closely spaced parallel glass plates. The water has a much higher viscosity than the air. The water undergoes a flow which is driven by pressure gradients. The pressure variations are produced by surface tension and the varying curvature of the interface. We are interested in asking how a mass of water can divide into two disconnected pieces. In [1], we argued that just before breakup there would be a thin bridging region which could be described by a variant of the lubrication approximation. We then looked at how the bridge could get narrower and narrower and finally pinch off at infinite time.

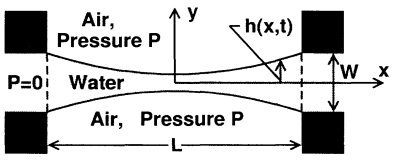

FIG. 1. Setup of the problem solved in this paper. Given is a sketch of the thin neck. Here the neck is symmetrical. A schematic picture showing the system setup and boundary conditions is given. The heavy lines are walls which separate the two fluids. The length L is much greater than length W. In this case we can equivalently imagine that there is a slip wall on the plane of symmetry. Our variable is $h(x,t)$.

In this paper we are concerned with pinch-offs that occur at finite time. The form of the hydrodynamic flow in the bridge is described by analytical arguments and computer simulations. In one limit, we compare the asymptotic behavior near the pinch with a matched asymptotic expansion.

Later in this section we derive the appropriate form of the lubrication approximation [6] to describe the thin bridge. The approximation takes into account inertial effects since flow through a narrow pinch tends to produce sufficiently high velocities to have a qualitative significance. With inertia, the approximation is a pair of nonlinear differential equations for the velocity and thickness of the material in the bridge. If the inertial parameter, called ρ, is set to zero, the approximation reduces to the one used in the previous paper [1]. Section II details the specific models to be studied and describes the numerical methods used. Two particular situations with finite-time touchdown are studied using simulation in Sec. III, one with $\rho=0$ and one with a small value of ρ. The re-

sults differ qualitatively from one another. The final section of the paper presents asymptotic analyses which describe and, in part, explain the numerical results.

In the quasi-two-dimensional Hele-Shaw system, the gap between the two glass plates is so thin that the velocity of water is quite parallel to the plates. On these plates, no-slip boundary conditions are realized, and the water flow is considered to be in a viscosity-dominated or low-Reynolds-number situation. Under these conditions, we assume that the velocity profile in the direction perpendicular to the plate is a parabola everywhere. From this we conclude that the viscosity term in the Navier-Stokes equation is proportional to the depth-averaged average velocity parallel to the plates, $\mathbf{v}$. In Eq. (2) below we also replace other terms related to velocity in the Navier-Stokes equation by this average velocity to retain approximately the effect of inertia. After proper scaling, $\mathbf{v}$ satisfies

$$\rho(\mathbf{v}_t+(\mathbf{v}\cdot\nabla)\mathbf{v})+\mathbf{v}+\nabla p=\mathbf{0}\ , \tag{1}$$

where the pressure p is presumed to depend only upon the coordinates x,y along the plates and ρ is a parameter. Later this equation is used in cases in which the Reynolds number is not always small because we hope it will give us qualitatively the correct picture of the interface dynamics of our system. The previous Hele-Shaw model is regained when $\rho=0$. Nonzero ρ corresponds to a case where inertial effects cannot be ignored. For simplicity we assume that both the viscosity and mass of the air are negligible. Then the pressure within the air may be considered to be independent of position [3].

An experiment in a Hele-Shaw cell was performed recently and indicates that droplets do break up in finite time [4], though it is not clear how important a role is played by the actual three-dimensional nature of the cell. In this paper we will not try to examine the details of this experiment; instead we will investigate whether, under the simplifications we have just made, the thin neck of a droplet in the Hele-Shaw cell will be able to break up in finite time.

The change in topology of the fluid in a Hele-Shaw cell was studied recently by Shelley, Goldstein, and Pesci [5]. They considered a situation in which the development of the singularity was driven by gravitational forces which result if the cell is tilted instead of horizontal.

A. Derivation of lubrication approximation

Further simplifications can be made since the width of the fluid neck is very thin. A standard lubrication approximation [6] will be applied to this thin neck region. We will limit ourselves to symmetrical neck cases since we believe they are physically more stable. For such a symmetrical neck, one variable $h(x,t)$ is enough to describe its shape, where x describes distance along the symmetry line, t is the time, and $2h$ is the thickness of the interface at position x.

The lubrication approximation is based on the assumption that the fluid system we are studying is a viscosity-dominated system and the interface is very thin so that we can treat the pressure as a function of x only. Thus the flow velocity will mainly point in the x direction and its x component, which we denote by v, satisfies

$$\rho(v_t+vv_x)+v+p_x=0\ . \tag{2}$$

Therefore the total current of particles j is velocity times height

$$j=vh\ , \tag{3}$$

and the continuity equation gives

$$\partial_t h+\partial_x j=0\ . \tag{4}$$

The last simplification is that we will replace the curvature κ in the x,y plane by h_{xx} because we are studying a very thin neck:

$$\kappa=\frac{h_{xx}}{(1+h_x^2)^{3/2}}\approx h_{xx}\ .$$

This approximation enables us to connect the pressure inside and outside of the viscous fluid by

$$p=P(t)-\tau h_{xx}\ , \tag{5}$$

where $P(t)$ is the pressure of the air.

If we put together Eqs. (1)–(5) and make proper rescaling, we will get the following set of equations:

$$\begin{aligned} &h_t+(vh)_x=0\ ,\\ &\rho(v_t+vv_x)+v+p_x=0\ ,\\ &p+h_{xx}-P(t)=0\ . \end{aligned} \tag{6}$$

When $\rho=0$ (inertia is neglected), we can replace this by

$$h_t+(hh_{xxx})_x=0\ . \tag{7}$$

Henceforth we limit ourselves to studying the models defined by Eqs. (6) and (7).

B. Zeros imply singularities

For our models a neck breakage implies that there are singularities in the solutions in the sense that some derivatives blow up. The following argument shows that this is the case. The argument uses the system from Eq. (6), but since it applies even when $\rho=0$, the result is valid for (7).

Let $x_{\min}(t)$ be the position of the minimum of $h(x,t)$ in x. The minimum value of h at time t is $h_{\min}(t)=h(x_{\min}(t),t)$. From Eq. (6) we know that

$$\frac{d}{dt}\ln(h_{\min})=-W(t),\quad W(t)=v_x(x_{\min}(t),t)\ . \tag{8}$$

If $h_{\min}$ approaches zero at any finite time t_c, the x derivative of v must have a very strong singularity—the integral of $W(t)$ up to t_c must diverge. Thus a zero in $h(x,t)$ implies a singularity in the x derivative of v.

II. SIMULATIONS AND LOCAL ANALYSIS

Imagine that we have a common of fluid of finite thickness and gradually increase the outside pressure to squeeze (see Fig. 2). There is no doubt that at late time

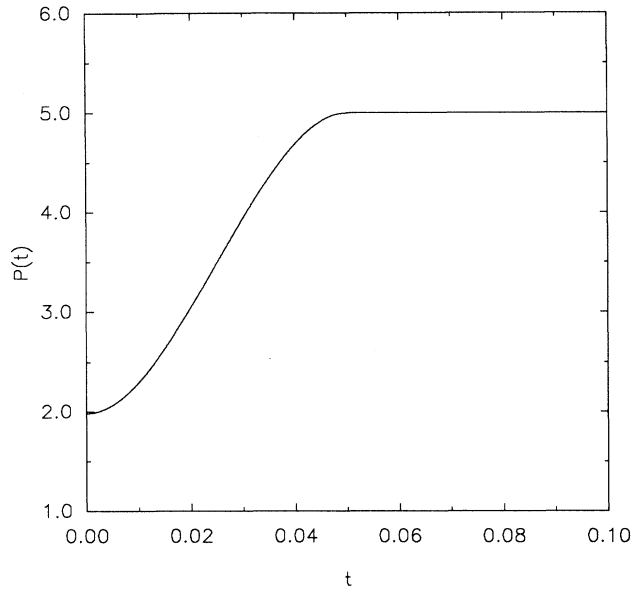

FIG. 2. $P(t)$, pressure field outside of the viscous fluid.

the minimum of thickness $h(x,t)$ of the neck will always decrease if we squeeze it very hard. In a previous paper [1] we found that for some initial conditions, the thickness $h(x,t)$ of the neck goes to zero as time tends to infinity; here we study two cases in which $h(x,t)$ reaches zero in finite time.

A. Models

Bearing the physical picture of our system (see Fig. 1) in mind, we impose the following boundary conditions for our equations. We consider $h(x,t)$ in a finite interval $-1<x<1$. At the two end points, we demand that $h(\pm 1,t)=1$ for all the time. The reference points of pressure are also chosen at the two ends points $-x=\pm 1$; we set the pressure inside the water to be zero at these two positions. The pressure in the air is kept to be $P(t)$. From Eq. (5) we see that the boundary conditions can be stated as follows:

$$h(\pm 1,t)=1, \quad h_{xx}(\pm 1,t)=P(t) \tag{9}$$

for $t\geq 0$. Here $P(t)$ is a dimensionless version of the pressure in the air. If $P>0$, the air is pushing on the water. There is a tendency for the column of water to thin. If $P<0$, the column has a tendency to bulge at the center. Note that there is no separate boundary condition for v. For the cases we study in this paper $P(t)$ will be gradually increased to a positive constant and kept at that constant for the rest of the time.

The initial conditions used here are that $h(x,0)$ is in a nonsingular equilibrium state and the initial velocity field is zero everywhere. Specifically, we take $P(0)$ to be in the interval (0,2) and define h and v initially by

$$h(x,0)=1-\frac{P(0)}{2}(1-x^2), \quad v(x,0)=0 . \tag{10}$$

B. Simulational methodology

The numerical method used in our simulations is a conventional finite-difference method. It is an implicit, two-level finite-difference scheme based on central differences except for the convective term vv_x, which is upwinded. For the $\rho=0$ case we compared simulation results obtained from the finite-difference method with those of the finite-element method in the previous paper and found that they agreed quite closely.

We consider the case of solutions to Eq. (6) that are symmetric about $x=0$. Symmetry in the initial conditions is preserved by the evolution, so $h(x,t)$ and $p(x,t)$ are even and $v(x,t)$ is odd about $x=0$. This symmetry allows us to work only on half the interval. Discretize the interval [0,1] by the N mesh points,

$$0=x_1<x_2<\cdots<x_N=1 .$$

At each computational time the height and pressure $h(x,t)$ and $p(x,t)$ are approximated by arrays h_i and p_i, $i=1,\ldots,N$, and the velocity is approximated by v_i, $i=1,\ldots,N-1$. The h_i and p_i values are associated with the point x_i, while v_i is the computed velocity at the center of the interval $(x_i+x_{i+1})/2$. These associations are indicated in the following picture:

Adopt the following notation:

$$\begin{aligned}
&\Delta x_{i+(1/2)}=x_{i+1}-x_i ,\\
&x_{i+(1/2)}=\tfrac{1}{2}(x_{i+1}+x_i) ,\\
&\Delta x_i=x_{i+(1/2)}-x_{i-(1/2)} ,\\
&h_{i+(1/2)}=\tfrac{1}{2}(h_{i+1}+h_i) ,\\
&\partial h_{i+(1/2)}=(h_{i+1}-h_{i-1})/\Delta x_{i+(1/2)} ,\\
&\delta^2 h_i=(\partial h_{i+(1/2)}-\partial h_{i-(1/2)})/\Delta x_i .
\end{aligned} \tag{11}$$

The term vv_x is approximated using an upwinded difference quotient for $\frac{1}{2}(v^2)_x$, where the upwind direction is based on v. This approximation is denoted $\frac{1}{2}\delta_u(v^2)$ and is defined as follows:

$$\delta_u(v^2)_i=\begin{cases}(v_{i+1}^2-v_i^2)/(x_{i+1+(1/2)}-x_{i+(1/2)}), & 0\leq v_i\\ (v_i^2-v_{i-1}^2)/(x_{i+(1/2)}-x_{i-(1/2)}) & \text{otherwise}\end{cases} . \tag{12}$$

For simplicity we describe the difference scheme in space first and later indicate the time discretization. We replace the equations in (6) as follows:

$$(h_i)_t+(h_{i+(1/2)}v_i-h_{i-(1/2)}v_{i-1})/\Delta x_i=0 , \tag{13}$$

$$\rho[(v_i)_t+\delta_u(v^2)_i]+v_i+\partial p_{i+(1/2)}=0 , \tag{14}$$

$$p_i+\delta^2 h_i-P(t)=0 . \tag{15}$$

The boundary conditions are imposed by setting $h_N=1$, $p_N=0$, and using the symmetry at $x=0$.

The above set of differential-algebraic relations is discretized in time using a simple two-level scheme. In advancing from time t to time $t+dt$ the time derivative terms are replaced by difference quotients involving the solution at the old time level (time t) and the as yet unknown solution at the new time level (time $t+dt$). The other terms are evaluated using a weighted average of the solution at the two time levels; we typically used a weight of $\theta=0.55$ on the advanced time level and $1-\theta=0.45$ on the old time level.

The fully discrete system is a set of nonlinear equations at each time level, and these equations were solved using Newton's method. The Jacobi matrix has all of its nonzero entries very close to the diagonal if one chooses an appropriate order for the computational unknowns, and the solution of the linear equations in Newton's method is not a dominant expense.

The time steps used in the solution of the discrete scheme were chosen dynamically so as to control several aspects of the simulation. When any constraint was violated the step was rejected and tried again with a smaller step size. If all the constraints were easily being met (and had been so for several steps) the step size was increased by about 20% on the next step. There was a constraint based on local time truncation, and another which assured that no step was accepted on which the minimum of h decreased by more than 10%. There was also a step constraint which assured that the correction on the first iteration of Newton's method was a very small fraction of the change over the step, where the initial guess at the change was the change over the previous step, corrected for any difference in dt's. This last constraint allowed us to conduct most of our experiments using only one Newton iteration per time step.

The spatial grids used were highly graded so that they were very fine near the singular points and less fine in other parts of the region. The location of the fine grid was a manual process which involved examining a sequence of finer and finer meshes. The meshes used had locally constant Δx_i's and the Δx_i's were increased or decreased by a factor of 2 at any point where they were changed. (In fact all the Δx values used were negative powers of 2.)

III. RESULTS OF SIMULATION

In this section we discuss the numerical simulation results in detail. We observed different behavior for the no-inertia case and the inertial case; these two cases are treated in separate subsections.

A. Finite-time singularity in no-inertia case

We present evidence of finite-time singularity in the solutions of Eq. (7). We have seen finite-time singularities with several different initial conditions but will exhibit one case in detail.

The initial condition we used in our simulations for no-inertia case is the following:

$$h(x,0)=1-\frac{P_{\text{initial}}}{2}(1-x^2)\ , \tag{16}$$

where P_{initial} is a constant less than 2.

The outside pressure field $P(t)$ changes with time as shown in FIg. 2. The specific formula for the pressure is

$$P(t)=\begin{cases} P_{\text{initial}}+(P_{\text{final}}-P_{\text{initial}})(3-2s)s^2 & \text{if } 0<s<1 \\ P_{\text{final}} & \text{if } s>1\ . \end{cases} \tag{17}$$

where $s=t/0.05$.

In the case we want to examine now, $P_{\text{initial}}=\frac{127}{64}$, $P_{\text{final}}=5$. (The only change from our previous study [1] is that earlier we used $P_{\text{initial}}=P_{\text{final}}=5$.) In Figs. 3 and 4 we plot $h(x,t)$ at different times. As time increases, h changes its shape from initially a parabola with a minimum at $x=0$ to a shape with two minima setting symmetrically on both sides of x axis. Dramatic things happen to $h_{\min}(t)$ (see Fig. 5). In contrast to our previous cases, now the minimum of $h(x,t)$ decreases to zero in finite time. At first, the minimum of $h(x,t)$ lies at $x=0$, $h_{\min}$ increases and reaches a maximum around $t_c-t\approx 0.05$. After $t_c-t\approx 0.06$ the minimum of h moves away from the center. Thereafter $h_{\min}$ goes down to zero monotonously. Around $t_c-t\approx 0.0008$, $h_{\min}$ decreases very fast. The dropping then becomes slower but the curve continues to go down and reaches zero at $t_c\approx 0.076\,326$. It is found that after $t_c-t\approx 0.0008$ the solution of our system begins to show self-similar properties.

The behavior of the curve for t very close to t_c or after $t_c-t\approx 0.0008$ is plotted in Fig. 6. The t_c is adjusted as a parameter to get the straightest line in the plot of $(t_c-t)/\sqrt{h_{\min}}$ versus $\log_{10}(t_c-t)$. Our matched asymp-

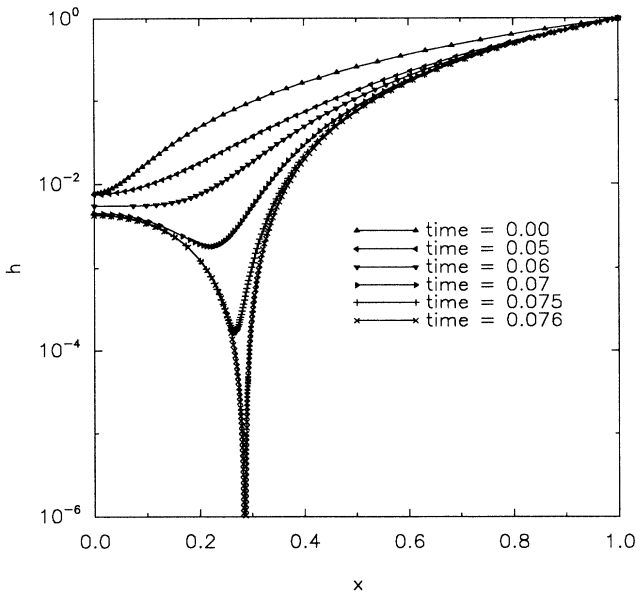

FIG. 3. Behavior of $h(x,t)$ in the case where $\rho=0$ and the pressure field outside of the water is smoothly increased from $\frac{127}{64}$ to 5. h becomes singular. Logarithm of the solution for $h(x,t)$ is shown for selected early times. Only the region $0<x<1$ is shown because the curves are symmetrical about $x=0$.

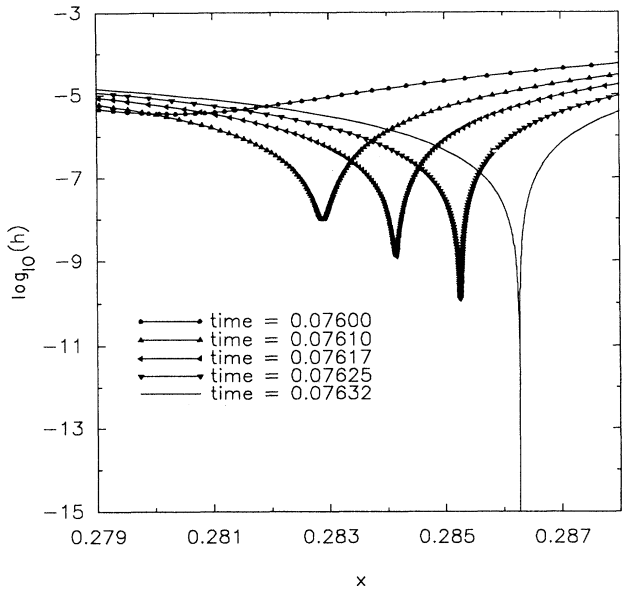

FIG. 4. An enlargement of the small-h region of Fig. 3 ($\rho=0$), carried to later times.

totic solution (see below) suggests that this curve should be a straight line. Our best power-law fit of $\sqrt{h_{\min}}$ versus t_c-t is checked in this figure, too. The ratio between $(t_c-t)^{1.21}$ and $\sqrt{h_{\min}}$ goes to a constant when $t\to t_c$. Limited by the round-off error of our computer, we cannot approach t_c very closely, with $t_c-t\sim 10^{-6}$ approximately the limit we can reach by doing double-precision calculations on a SUN computer workstation. Around $t_c-t\sim 10^{-6}$ we begin to see oscillations in $h_{\min}$. Our best power-law fit is

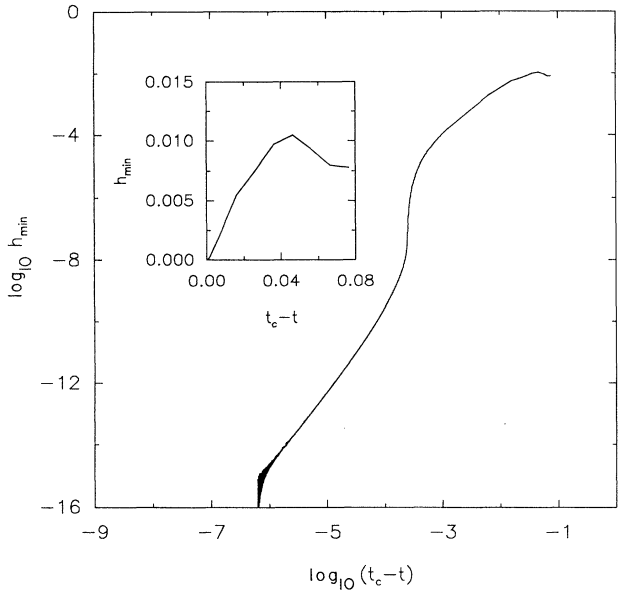

FIG. 5. Plot of $\log_{10}h_{\min}$ vs $\log_{10}(t_c-t)$ for $\rho=0$. Here $t_c\approx 0.076\,326$. The inset shows early behavior of $h_{\min}$.

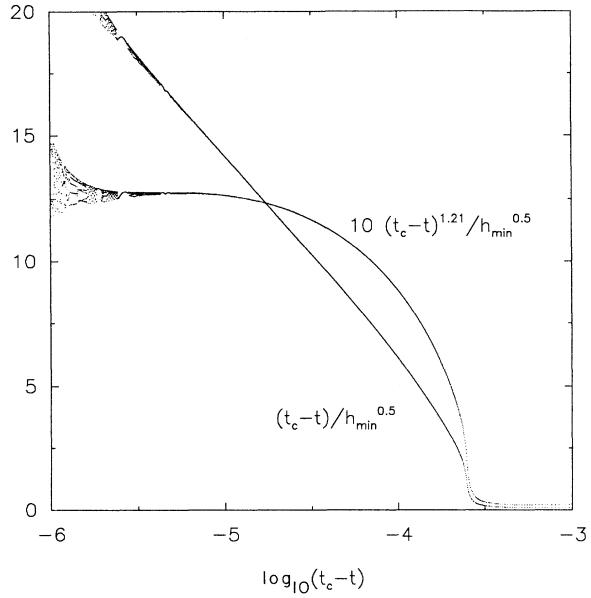

FIG. 6. Two ratios are plotted against $\log_{10}(t_c-t)$ for $\rho=0$. One is $R_1=(t_c-t)/\sqrt{h_{\min}}$. The other is $R_2=10(t_c-t)^{1.21}/\sqrt{h_{\min}}$. Here t_c is adjusted to get as big as possible a range of straight line in the R_1 plot. Notice that over a big range R_1 is very close to a straight line and R_2 approaches a constant when $t\to t_c$.

$$h_{\min}\sim(t_c-t)^{2.42\pm0.05}\ , \tag{18}$$

which is a good approximation in the range $10^{-6}\lesssim t_c-t\lesssim 10^{-4}$. But a better fit is

$$h_{\min}\sim\left\{(t_c-t)\Big/\log_{10}\left[\frac{t_c-t}{t_s}\right]\right\}^2\ , \tag{19}$$

as $t\to t_c$. Here $t_s\approx 0.0007$ is a time scale indicating when the self-similar solution becomes the dominant term in $h_{\min}$.

There are several other interesting quantities in this problem which deserve careful study. Let us examine them one by one.

The first one is the current at the minimum point of $h(x,t)$, $J_{\min}(t)=j(x_{\min}(t),t)$. From Fig. 7 one can immediately find that now $J_{\min}(t)$ goes to zero in finite time. When the outside pressure becomes constant ($t\geq 0.05$), the current of the water gradually forms a new minimum around $x_{\min}$ and j at this new minimum goes to zero in finite time (see Fig. 7). This feature is certainly different from what we observed in our previous studies, for which, in the pinch region, j went to zero only at infinite time. The zero in j will be a crucial fact in understanding our solutions. Next we performed a power-law fit to find the relation between $J_{\min}(t)$ and t_c-t. Here we use the t_c we got from Fig. 6. The fit tells us that as $t\to t_c$, the asymptotic relation between j and t_c-t is

$$J_{\min}(t)\sim(t_c-t)^{1.19}\ . \tag{20}$$

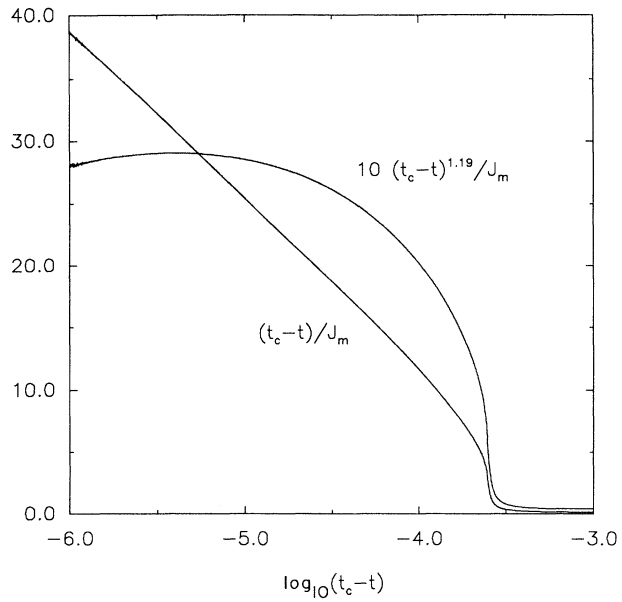

FIG. 7. Two ratios are plotted against $\log_{10}(t_c-t)$ for $\rho=0$. One is $R_3=(t_c-t)/J_{\min}$, where $J_{\min}$ is the current j at $x_{\min}$. The other is $R_4=10(t_c-t)^{1.19}/J_{\min}$. t_c is the same as that in Fig. 6. Notice that over a big range R_3 is very close to a straight line and R_4 becomes approximately a constant when $t\to t_c$.

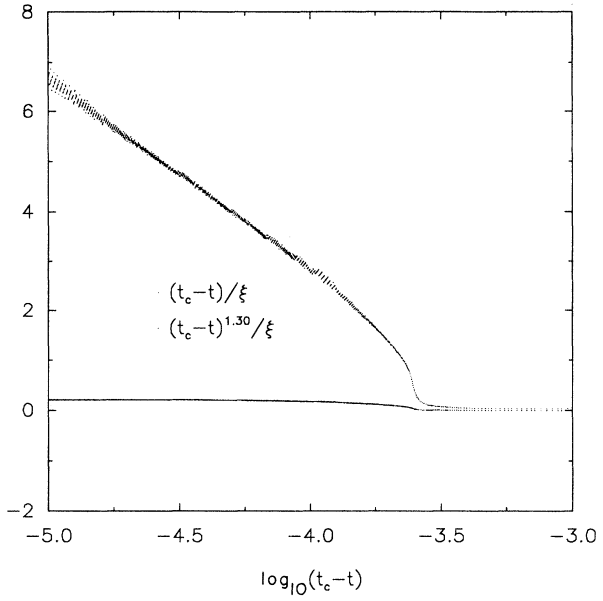

FIG. 8. Plot of $R_5=(t_c-t)/\xi$ and $R_6=30(t_c-t)^{1.30}$ vs $\log_{10}(t_c-t)$ for the no-inertia case at late times ($\rho=0$).

The prediction from the matched asymptotic solution is that $J_{\min}(t)$ should scale like $(t_c-t)/\log_{10}[(t_c-t)/t_s]$ for very late time. Both descriptions of $J_{\min}(t)$ are examined in Fig. 7 where $R_3=(t_c-t)/J_{\min}$ and $R_4=10(t_c-t)^{1.19}/J_{\min}$ are plotted against $\log_{10}(t_c-t)$. If the power-law fit is correct, R_4 should be a constant. If the matched asymptotic solution is right, we shall see R_3 be a straight line in Fig. 7. From Fig. 7 one sees that our numerical results agree with the prediction given by the matched asymptotic solution over a wider range than just a simple power law.

Another interesting quantity is the width of pinch region $\xi(t)$. It is defined as the distance between two points where h is twice as big as $h_{\min}$. These two points sit on different sides of $x_{\min}$ and serve as markers for the pinch region. A power-law fit and a fit suggested by the matched asymptotics are illustrated in Fig. 8. Our data suggest that roughly

$$\xi(t)\sim(t_c-t)^{1.30\pm0.05}\ , \tag{21}$$

and that ξ can be better described by a prediction of the matched asymptotic solution,

$$\xi(t)\sim(t_c-t)\Big/\log_{10}\left[\frac{t_c-t}{t_s}\right]\ . \tag{22}$$

The third interesting quantity is another length scale in this problem, the width of an intermediate region $L^{\pm}(t)$. It is related to the current j (see Fig. 9). It can be measured in the following way: find the minimum of the current (for late time it is at $x_{\min}$). From this minimum search the right (left) side to find the first point where j is twice as big as $J_{\min}$; the distance between this point and the minimum is $L^{+}(t)$ $[L^{-}(t)]$. These two points set the limits of the intermediate region. Again we illustrate fits graphically; we plot $\sqrt{t_c-t}\,/L^{\pm}$ and $(t_c-t)^{0.54}/L^{\pm}$ versus $\log_{10}(t_c-t)$ in Fig. 10, where power 0.54 ± 0.05 is our best fit from a log-log plot of $L^{\pm}$ versus t_c-t. Figure 10 indicates that this fit works for $10^{-6}\lesssim t_c-t\lesssim 10^{-4}$.

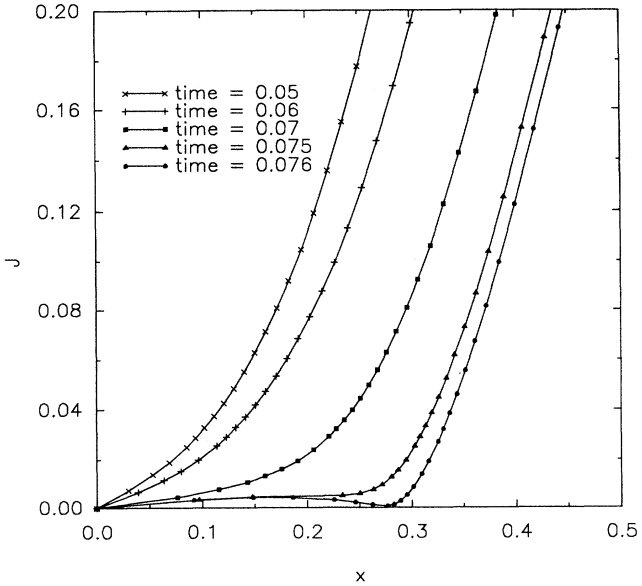

FIG. 9. The current $j=hh_{xxx}$ at various times for the case $\rho=0$ and the pressure field outside of the water is smoothly increased from $\frac{127}{64}$ to 5. It forms a local minimum at $x_{\min}$ lately. The current does go to zero at finite time.

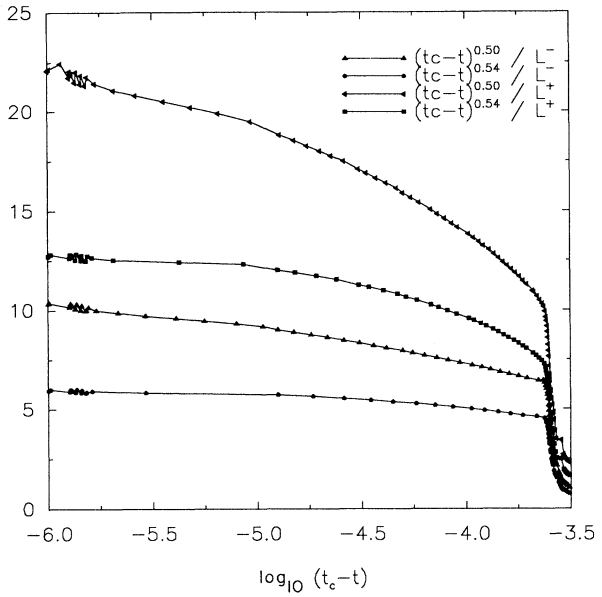

FIG. 10. Plot of $\sqrt{t_c-t}/L^{\pm}$ and $t_c-t^{0.54}/L^{\pm}$ vs $\log_{10}(t_c-t)$ for the no-inertia case at late times ($\rho=0$).

The asymptotic analysis predicts a power 0.5, so our numbers agree with the prediction.

The fourth interesting quantity is $x_{\min}(t)$, the x value at which $h(x,t)$ attains its minimum. The plot of $x_{\min}(t)$ versus t is very close to a straight line which implies that when $t\rightarrow t_c$, the minimum of $h(x,t)$ moves at a constant velocity.

The simple asymptotic behavior of the pinch region and intermediate region is shown in Figs. 11 and 12. Figure 11 plots $h/h_{\min}$ versus $(x-x_{\min})/\xi$. For $-2\xi\lesssim x-x_{\min}\lesssim 2\xi$ we see a beautiful superposition of h from our late-time data. Similar superposition for the intermediate region is demonstrated in Fig. 12. There $j/J_{\min}$ is plotted as a function of $(x-x_{\min})/L^{\pm}$ for several different late times.

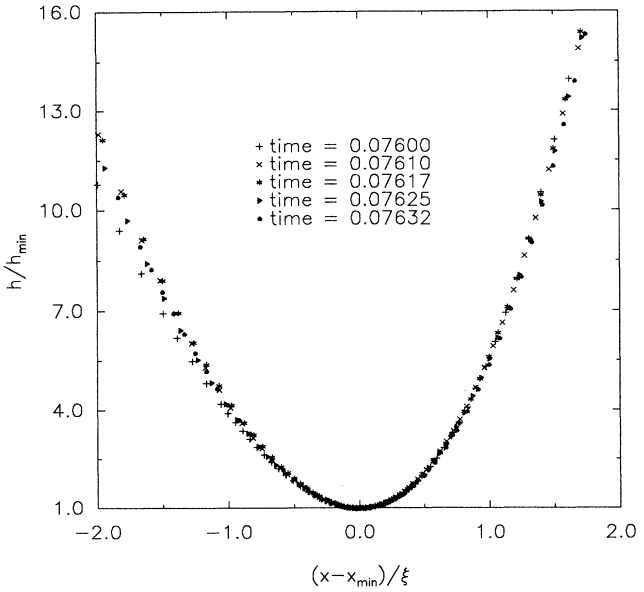

FIG. 11. Late-time shape of the pinch region for the case where $\rho=0$ and the pressure field outside of the water is smoothly increased from $\frac{127}{64}$ to 5. Notice that the shape of the pinch region is not symmetric about its minimum. The x axis is $(x-x_{\min})/\xi$ and the y axis is $h/h_{\min}$.

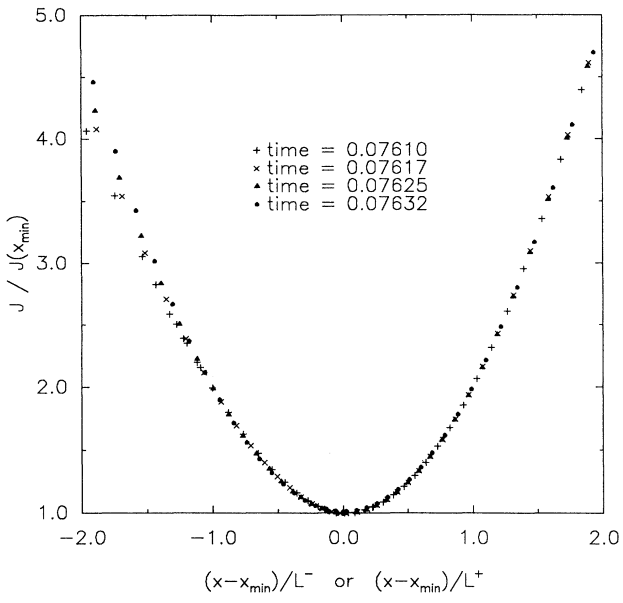

FIG. 12. Late-time shape of the intermediate region for the case where $\rho=0$ and the pressure field outside of the water is smoothly increased from $\frac{127}{64}$ to 5. Notice that the shape of the intermediate region is not symmetric about its minimum. The x axis is $(x-x_{\min})/L^{\pm}$ and the y axis is $j/J_{\min}$.

At t_c, the lowest diverging x derivative of $h(x,t)$ is h_{xxx}. The shape of the interface for $|x-x_{\min}|\gg\xi$ around $x_{\min}(t_c)$ is very close to two parabolas, which are tangent to the x axis at $x_{\min}(t_c)$ (see Fig. 11). The pressure field inside the water, or $P(t)-h_{xx}$, is shown in Fig. 13. This figure shows that within the pinch region the pressure jumps from one value to another.

B. Finite-time singularity in inertial case

The initial conditions used in this case are the same as Eq. (16). The pressure field outside the water is changed with time according to Eq. (17) (see Fig. 2).

We have tried several different ρ in our simulations. The one we are going to discuss in detail is $\rho=0.005$. Figures 14–19 show us the overall plots of $h(x,t)$ versus x,$p(x,t)$ versus x, and $v(x,t)$ versus x both for early times and late times. Again $h(x,t)$ reaches zero in finite time. Now both the velocity and the pressure field diverge in finite time. We begin our discussion with the $h_{\min}(t)$ versus the t plot (see Fig. 20). The minimum of $h(x,t)$ does not change very much until it reaches $t\approx 0.01$. The behavior of $h_{\min}(t)$ for $t\leq 0.05$ is quite close to that in the $\rho=0$ case. Then it bounces back and goes down. Once again $h_{\min}(t)$ drops to zero monotonously in finite time. The critical time extrapolated from

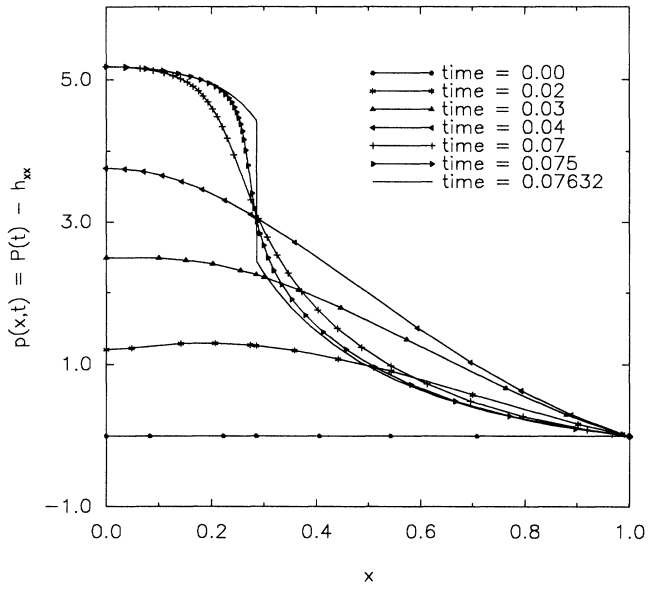

FIG. 13. Pressure field p or $P(t)-h_{xx}$ at various times. This is obtained from a $\rho=0$ simulation with initial condition Eq. (17) and the pressure field outside of the water is smoothly increased from $\frac{127}{64}$ to 5. Notice p itself does not diverge. It has a jump around $x\approx 0.286\,274\,79\ldots$ when $t\to t_c$.

our data for the $\rho=0.005$ case is $t_c\approx 0.079\,81$. Figure 21 exhibits how $h_{\min}(t)$ changes with t when $t\to t_c$. Figure 21 can be fit via

$$h_{\min}(t)\sim(t_c-t)^{0.766\pm 0.050}\ ,$$

when $t\to t_c$ from below.

Good power-law fits are found in the behaviors of $x_{\min}(t)-x_{\min}(t_c)$ versus (t_c-t) (see Fig. 22); $J_{\min}(t)$ versus (t_c-t) (see Fig. 23); $\xi(t)$ versus (t_c-t) (see Fig. 24); $p(x_{\min}(t))$ versus (t_c-t) (see Fig. 25); and $v(x_{\min}(t),t)$ versus (t_c-t) (see Fig. 26) when $t\to t_c$. Define

$$h_{\min}(t)\sim(t_c-t)^{\nu_1}\ , \tag{23}$$

$$\xi(t)\sim(t_c-t)^{\nu_2}\ , \tag{24}$$

$$x_{\min}(t_c)-x_{\min}(t)\sim(t_c-t)^{\nu_3}\ , \tag{25}$$

$$J_{\min}(t)\sim(t_c-t)^{\epsilon}\ , \tag{26}$$

$$v(x_{\min}(t),t)\sim(t_c-t)^{-\zeta}\ , \tag{27}$$

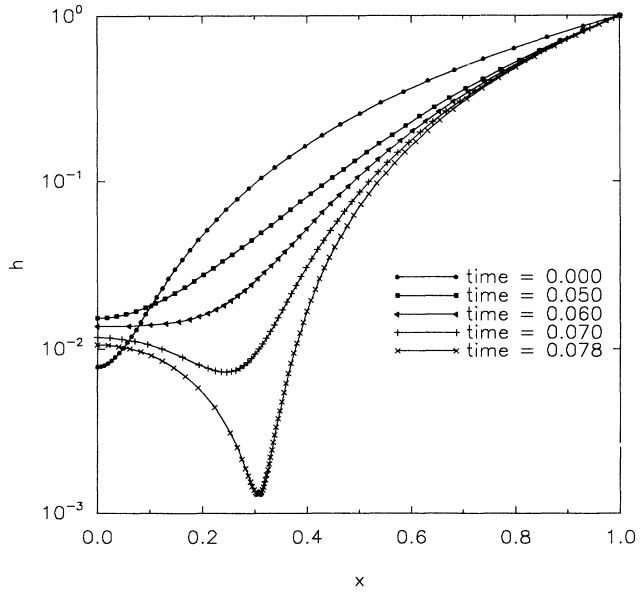

FIG. 14. Plot of $h(x,t)$ at early times for the $\rho=0.005$ case.

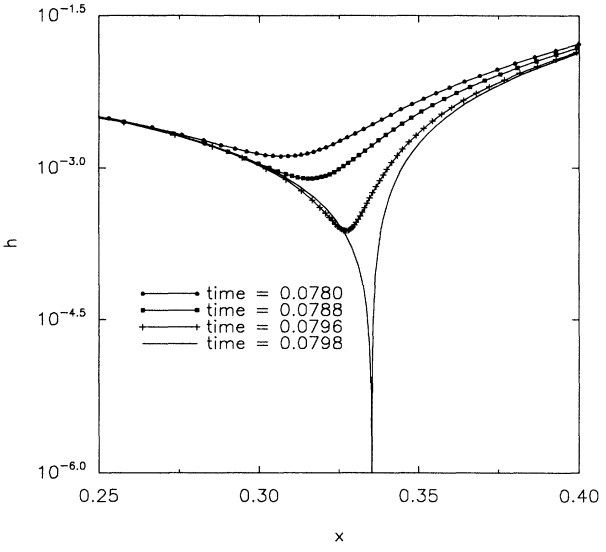

FIG. 15. Plot of $h(x,t)$ at late times for the $\rho=0.005$ case.

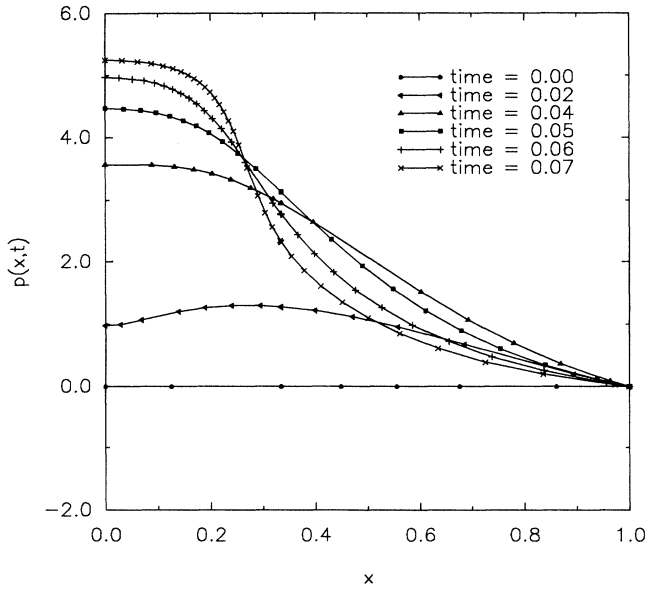

FIG. 16. Plot of $p(x,t)$ at early times for the $\rho=0.005$ case.

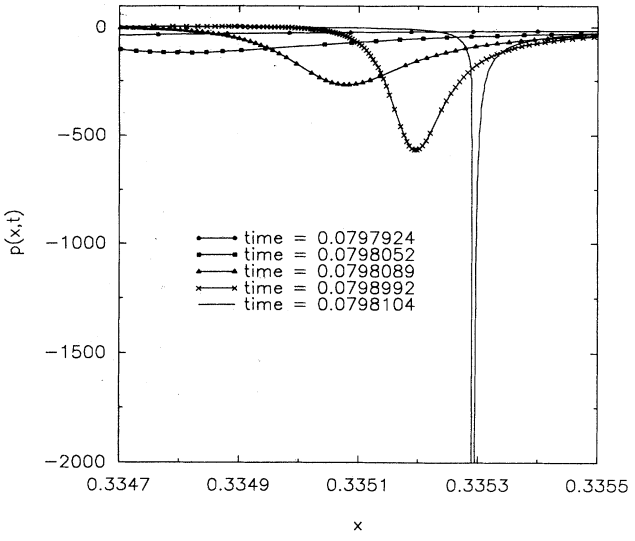

FIG. 17. Plot of $p(x,t)$ at late times for the $\rho=0.005$ case.

$$p(x_{\min}(t)) \sim -(t_c - t)^{-\theta} , \tag{28}$$

when $t \to t_c$. Our numerical results can be summarized in Table I.

It is worth pointing out the difference of the shape of the pinch region between the two cases. When $\rho=0$, we always see that when $L \gg |x - x_{\min}(t)| \gg \xi$ the pinch region is formed by two parabolas tangential to the x axis. This is no longer the case. Figure 27 shows the shape of the pinch region for the $\rho=0.005$ case. The ξ_l (ξ_r) is the distance from $x_{\min}$ to the first point on its left (right) side where h is twice as high as $h_{\min}$. From this figure we find that the right half of the pinch region is very close to a parabola, but not the left half. The shape of the left half

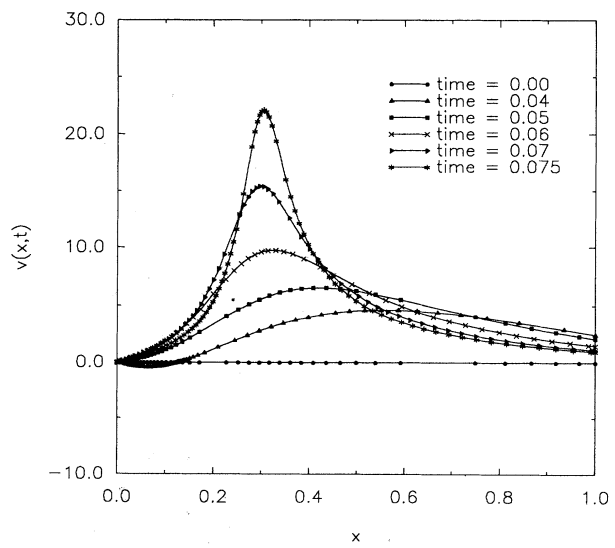

FIG. 18. Plot of $v(x,t)$ at early times for the $\rho=0.005$ case.

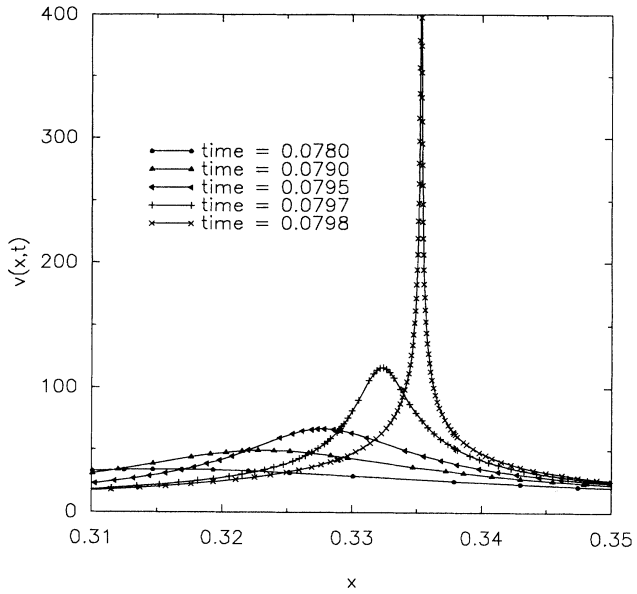

FIG. 19. Plot of $v(x,t)$ at late times for the $\rho=0.005$ case.

TABLE I. Table of critical indices for the $\rho \neq 0$ case.

Quantity	Index	Numerical value
$h_{\min}(t)$	ν_1	0.766±0.050
$\xi(t)$	ν_2	0.713±0.050
$x_{\min}(t_c) - x_{\min}(t)$	ν_3	0.684±0.050
$J_{\min}(t)$	ϵ	0.446±0.050
$v(x_{\min}(t),t)$	ζ	0.320±0.050
$p(x_{\min}(t))$	θ	0.642±0.050

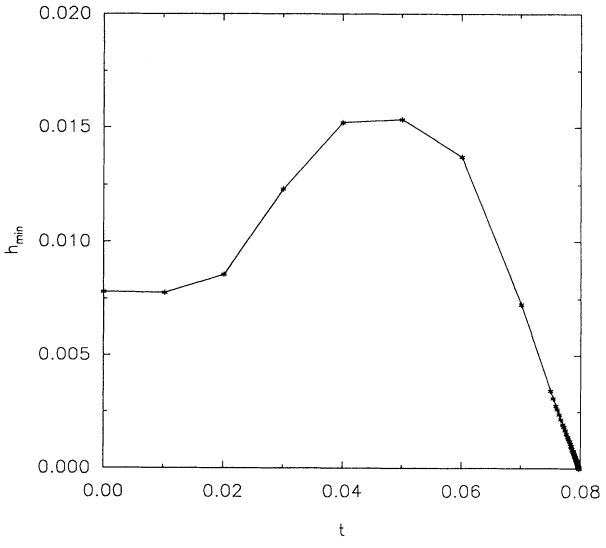

FIG. 20. Plot of $h_{\min}$ as a function of time for the $\rho=0.005$ case.

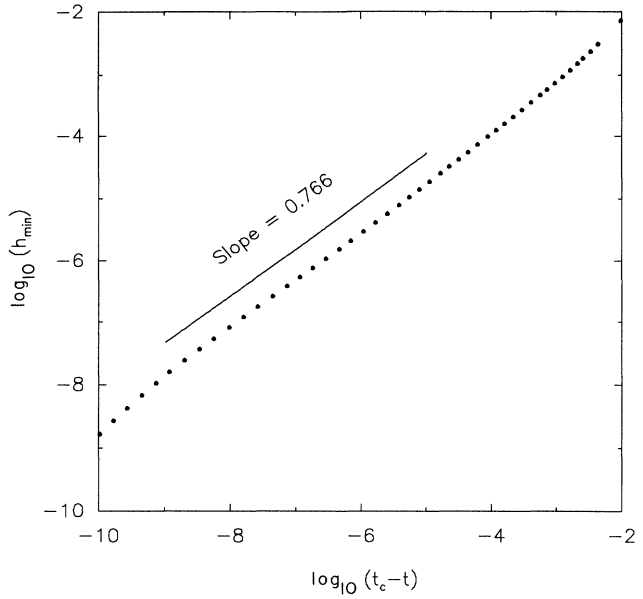

FIG. 21. Two ratios are plotted against $\log_{10}(t_c-t)$ for $\rho=0.005$. One is $R_1=(t_c-t)/\sqrt{h_{\min}}$. The other is $R_2=10(t_c-t)^{1.21}/\sqrt{h_{\min}}$. Here t_c is adjusted to get as big as possible a range of straight line in the R_1 plot. Notice that over a big range R_1 is very close to a straight line and R_2 approaches a constant when $t\to t_c$.

of the pinch region is close to a linear function when $(x_{\min}-x)\gtrsim\xi_l$.

This difference can be easily found from the plot of the pressure field inside the water, or $h_{xx}-P(t)$, too. Figure 25 provides clear evidence that the pressure field inside the water diverges when $x\approx 0.3353$.

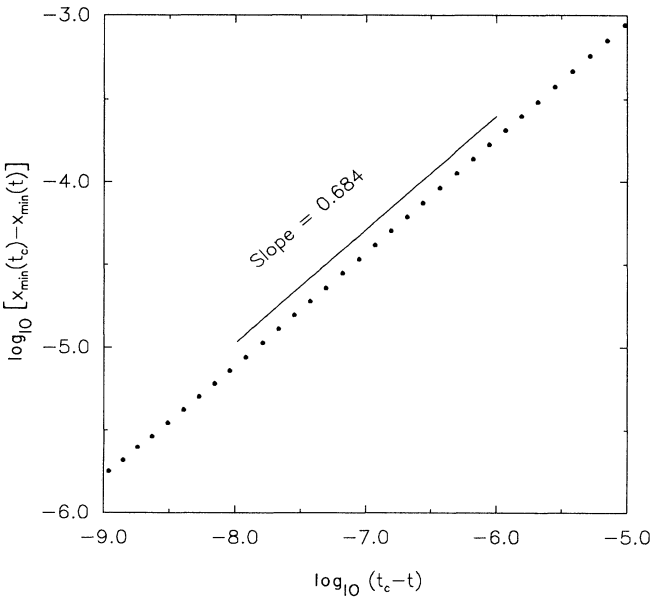

FIG. 22. Plot of $x_{\min}$ as a function of t at late time for the inertial case ($\rho=0.005$).

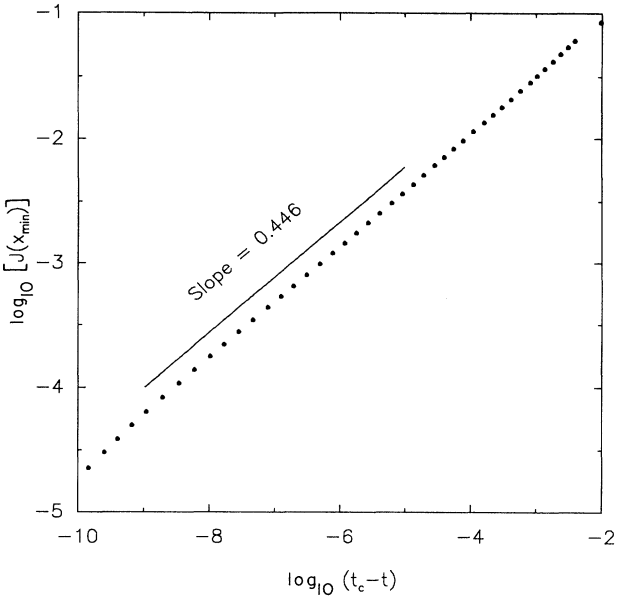

FIG. 23. Scaling of the current when $\rho\neq 0$ ($\rho=0.005$). The current at the pinch point $J_{\min}(t)$ is plotted vs t_c-t.

IV. SCALING ARGUMENT AND MATCHED ASYMPTOTIC SOLUTION

In this section we will first discuss an asymptotic solution of the $\rho\neq 0$ case, then construct a matched asymptotic solution which catches essential features we observed from simulations of the no-inertia case.

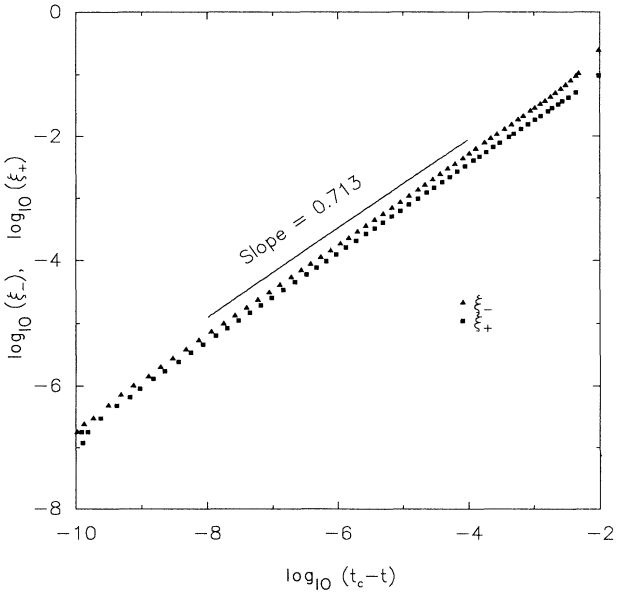

FIG. 24. Scaling of the width of the pinch region for $\rho=0.005$ case. The width of the pinch region ξ is plotted against t_c-t.

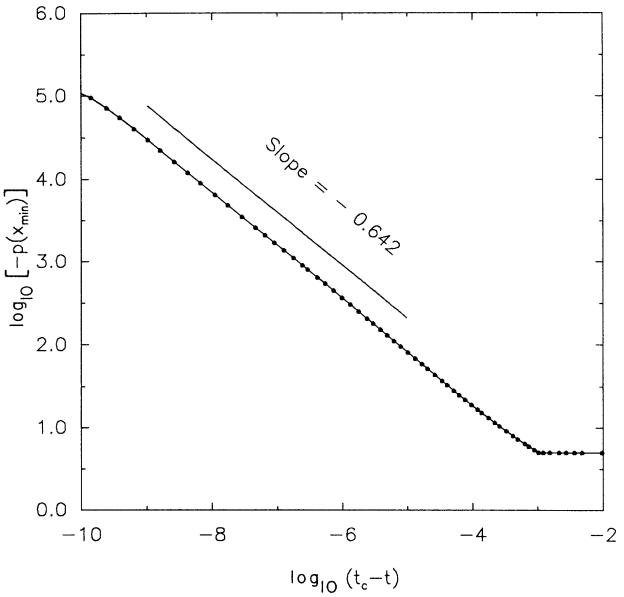

FIG. 25. Scaling of the absolute value of the pressure at the pinch point for $\rho \neq 0$ case ($\rho=0.005$). $|p(x_{\min}(t))|$ is plotted vs $t_c - t$.

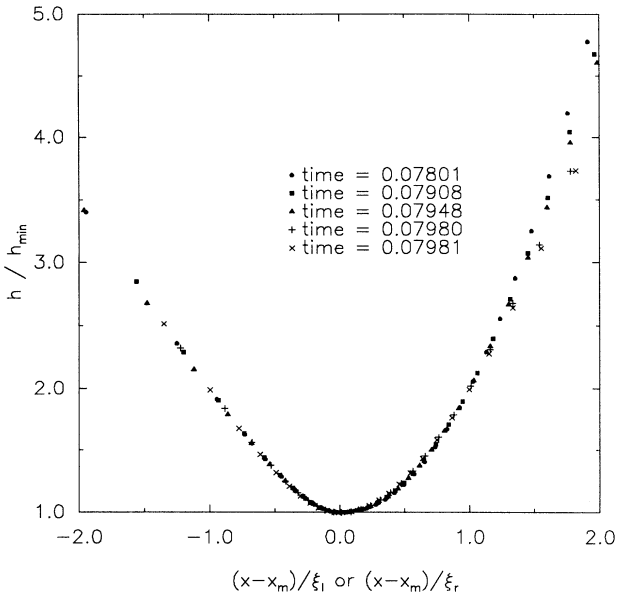

FIG. 27. Plot of pinch region shape for the $\rho \neq 0$ case ($\rho=0.005$).

A. Asymptotic analysis for $\rho \neq 0$

Next we turn to a rough asymptotic analysis which describes the situation in which ρ is not zero. We start from Eqs. (6) to get

$$h_t + (vh)_x = 0 ,$$
$$\rho(v_t + vv_x) + v = h_{xxx} . \tag{29}$$

Let us assume a similarity solution centered about the point $a = x_{\min}(t)$ with typical velocity $u = v(x_{\min}(t), t)$ and length scale ξ. We write

$$h(x,t) = h_{\min}(t) H(\eta) , \tag{30}$$
$$v(x,t) = u(t) V(\eta) , \tag{31}$$
$$\eta = \frac{x-a}{\xi} . \tag{32}$$

For simplicity take $x_{\min}(t_c)=0$, and assume that $a/\xi = r$ is independent of time to get

$$\frac{\dot{h}_{\min}}{h_{\min}} H - \frac{\dot{\xi}}{\xi}(\eta + r) H_\eta + \frac{u}{\xi}(VH)_\eta = 0 ,$$
$$\frac{\dot{u}}{u} V - \frac{\dot{\xi}}{\xi}(\eta + r) V_\eta + \frac{V}{\rho} + \frac{u}{\xi} V V_\eta = \frac{h_{\min}}{\rho \xi^3 u} H_{\eta\eta\eta} . \tag{33}$$

We are interested in the behavior that these equations imply for large values of η so some terms can safely be ignored. To get a balance in these equations, neglect the V/ρ term, drop r, and assume that

$$\frac{u}{\xi} = \frac{1}{t_{c-t}} = \frac{h_{\min}}{\rho \xi^3 u} . \tag{34}$$

These results agree well with the scaling indices displayed in Table I. Then if we use the notation of Table I, we can write

$$-\nu_1 H + \nu_2 \eta H_\eta + (VH)_\eta = 0 ,$$
$$\zeta V + \nu_2 \eta V_\eta + V V_\eta = H_{\eta\eta\eta} . \tag{35}$$

[The rescaling of η that is implicit in the use of (34) without coefficients could leave a coefficient on $H_{\eta\eta\eta}$ but this term will be very small for large η.]

To make further progress we must assume that V be-

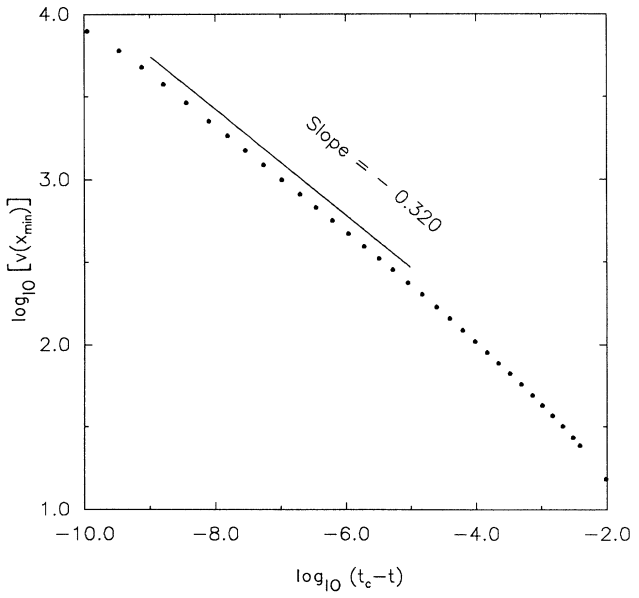

FIG. 26. Scaling of the water velocity at $x_{\min}$ for $\rho=0.005$. The water velocity at $x_{\min}$, $v(x_{\min}(t),t)$ is plotted vs $t_c - t$.

comes small for large values of η; as t approaches t_c the coefficient of V becomes very large, thus we need V to be small so that v will be moderate far from the singular point. For general values of the indices in Eq. (35), V will grow linearly with η. To avoid this unwanted outcome, we must assume that for large η, V is small and then notice that $H_{\eta\eta\eta}$ will be zero. Then H will be quadratic in η. We cannot see how to get balance with indices close to those in Table I if H grows like η^2, so we assume that H is linear in η; specifically,

$$H=\eta+A\eta^p+\cdots , \tag{36}$$

with $p<0$. Then, to make V small we assert that

$$\nu_1=\nu_2 , \tag{37}$$

so that the first equation of (35) now gives

$$VH=\frac{p-1}{p+1}\nu_1 A\eta^{p+1} ,$$

so that we obtain

$$V=\frac{p-1}{p+1}\nu_1 A\eta^p+O(\eta^{2p-1})+O(\eta^{3p-2}) , \tag{38}$$

which is small, as desired. In writing (38), we set a constant of integration equal to zero. The substitution of (38) into the second equation of (35) gives a linear growth of H for large η only if

$$\zeta+\nu_2 p=0 . \tag{39}$$

The growth η^p can only be obtained if the last correction term in (38) is of order η^{p-3}, so that we find

$$p=-\tfrac{1}{2} . \tag{40}$$

Put Eqs. (34), (37), (39), and (40) together and obtain

$$\nu_1=\nu_2=\nu_3=\tfrac{2}{3},\quad \zeta=\tfrac{1}{3} . \tag{41}$$

These results roughly agree with Table I. The disagreement may be due to logarithmic terms, which could be incorrectly treated by the analysis above. However, the difference is not so large as to rule out the values in (41).

B. Matched asymptotic solution for $\rho=0$ case

We are looking for a similarity solution to Eq. (7) which holds in the neighborhood of the pinch point. To find this kind of solution, define a new variable $g(x,t)$ by

$$h(x,t)=g_x(x,t) , \tag{42}$$

and write Eq. (7) as

$$g_t+g_x g_{xxxx}=0 . \tag{43}$$

We analyze the solution to Eq. (43) by looking at three regions.

(i) A very narrow pinch region in which $h(x,t)$ is very small but positive. In this region, centered at x equal to $a(t)=x_{\min}(t)$, we assume that, to leading order, the current in this region, $j(x,t)=-g_t(x,t)$, depends upon time but is independent of x. This assumption will be the basis of an asymptotic expansion in this inner region.

(ii) Two somewhat wider regions bordering on the pinch region. The region which lies at higher (lower) values of x than the pinch is described by the upper (lower) of a pair of signs, $+$ $(-)$. In these two regions, the lowest-order terms in $g(x,t)$ will be cubic in x, hence

$$g\sim A_{\pm}(x-a)^3 .$$

Then, as we have discussed before,

$$P-h_{xx}=P-3!A_{\pm}$$

is the pressure, assumed almost constant, in each of these regions. This assumption of constancy will permit an asymptotic expansion for these regions which can then be matched [7] to the solution near the pinch.

1. *Pinch region*

Start with the pinch region. Assume that the pinch region has a characteristic size $J(t)$, where J goes to zero at the critical time. (It turns out, as we see below, that J is the current.) Let $a(t)$ be the center of the pinch region and assume a solution of the form

$$g(x,t)=K(t)+J^3G(\eta)+a_tJ^4G^{(1)}(\eta)+J_tJ^4G^{(2)}(\eta)+\cdots . \tag{44}$$

Here we have written terms which successively decrease in magnitude when the similarity variable

$$\eta=(x-a)/J \tag{45}$$

is of order unity and when t is close to the critical time for pinch off t_c. Our basic expansion parameter is

$$\epsilon=t_c-t . \tag{46}$$

We assume that J goes to zero as ϵ goes to zero. Our assumption that the leading-order x-dependent term is the one of order J^3 is the assertion that the pressure, which is $P-g_{xxx}$, is finite at pinch off. Substitute expansion (44) in Eq. (43) and retain lowest-order terms, assuming that the time derivatives $(J^2)_t$ and $(aJ)_t$ both are much smaller than unity. The resulting equation is

$$JG_\eta G_{\eta\eta\eta\eta}=-K_t . \tag{47}$$

Here the right-hand side of Eq. (47) is the total current of fluid through the pinch region. For definiteness, assume that this current is positive for times earlier than the time of pinch off, and decreases toward zero at pinch off. Then J and $-K_t$ are each small quantities. To get a t-independent equation, define the scale factor J by

$$J=K_t . \tag{48}$$

Thus, J has the additional interpretation of being the current through the pinch. From Eq. (48), Eq. (47) becomes

$$G_\eta G_{\eta\eta\eta\eta}=1 . \tag{49}$$

Physically, we would like to see a situation in which the pressure changed abruptly within a distance of order J around the pinch, and then settled down in the two in-

termediate regions in two different constant values. To achieve this, we need the leading terms in the asymptotic expansions of the G as η goes to $\pm\infty$ to be of the form

$$G = A_{\pm}\eta^3 .$$

Using Eq. (49), we can then calculate higher-order terms in the form

$$G = A_{\pm}\eta^3 - \eta^2 \log_{10}(|\eta|)/6A_{\pm} + O(\eta[\log_{10}(|\eta|)]^2) . \tag{50}$$

The quantities $A_{\pm}$ in Eq. (50) must be positive in order that g_x be positive.

To match onto the intermediate regions, a higher-order analysis is required, which takes into account the effects of the time dependence of J and of a. The substitution of Eq. (44) into Eq. (43) gives equations of motion for $G^{(1)}$ and $G^{(2)}$. These, respectively, obey the two fourth-order inhomogeneous linear equations

$$G^{(1)}_{\eta\eta\eta\eta} + G^{(1)}/G^2_{\eta} = 1 , \tag{51}$$

$$G^{(2)}_{\eta\eta\eta\eta} + G^{(2)}/G^2_{\eta} = -(3G - \eta G_{\eta})/G_{\eta} . \tag{52}$$

For large values of $|\eta|$, these quantities have asymptotic expansions which are polynomially bounded in $|\eta|$. The expansions are performed by assuming that the right-hand side of each equation gives the leading contribution to the fourth derivative As a result, the expansions start off

$$G^{(1)} \to \eta^4/4! + O(\eta^3 \log_{10}(|\eta|)) ,$$

$$G^{(2)} \to -\eta^4 \log_{10}(|\eta|)/432A^2_{\pm} .$$

Put this all together and discover the approximate value, for large η, of $g(x,t)$. We write the result in terms of the coordinate y, which measures separation from the pinch point $y = x - a(t)$. The result is that, for y of order J,

$$g(x,t) = A_{\pm}y^3 + \{ -Jy^2 \log_{10}(|y|/J)/6A_{\pm} + K(t) + a_t y^4 \log_{10}(|y|/J)/432A^2_{\pm} \} + \cdots . \tag{53}$$

The grouping of terms in Eq. (53) points toward the next regions in which the y^3 terms will be the leading behavior, while to logarithmic accuracy, all the remaining terms will be of the same, higher, order.

2. *Intermediate regions I*

Next, we would like to fit this onto solutions which would be correct for larger values of $|y|$. The first term in (53) describes a pressure which is constant except for a jump at $y = 0$. Assume that this term dominates the solutions for larger $|y|$. Specifically, take the intermediate regions to have characteristic distance variables

$$\mu = y/L^{\pm}(t) , \tag{54}$$

with $L^{\pm}(t)$ being the width of each of these regions. We expect that $L^{\pm}(t)$ will go to zero at the critical time. In our work, we assume that $L^{\pm}(t)$ [or rather a power of $L^{\pm}(t)$] forms appropriate expansion parameters for the intermediate regions, when $\mu = y/L^{\pm}$ is of order unity. Specifically, in this section, we write an asymptotic expansion which we expect to be valid in some range of μ,

$$L \ll |\mu| \ll o(|\log_{10} L|) . \tag{55}$$

We write down an equation of motion for $R_{\pm}(\mu, L^{\pm})$, defined as

$$g(x,t)/(L^{\pm})^3 = A_{\pm}\mu^3 + R_{\pm}(\mu, L^{\pm}) , \tag{56}$$

in the form

$$R_{\mu\mu\mu\mu} = (-L_t L)(3 + L\partial_L - \mu\partial_{\mu})R/(3A\mu^2 + R_{\mu}) + a_t L . \tag{57}$$

Here, the $\pm$ symbols have been dropped temporarily to achieve a relative simplicity of notation. In addition, we expand R as

$$R_{\pm}(\mu, L^{\pm}) = L^{\pm}F_{\pm}(\mu) + (L^{\pm})^2 F^{(1)}_{\pm}(\mu) + \cdots . \tag{58}$$

To get a simple expansion for R, assume that the correction term R_{μ} in the denominator of Eq. (57) is a small correction, and all other terms as written contribute to the lowest order. Then Eq. (57) becomes

$$(F_{\pm})_{\mu\mu\mu\mu} = (-L^{\pm}_t L^{\pm})(4 - \mu\partial_{\mu})F_{\pm}/3A_{\pm}\mu^2 + a_t . \tag{59}$$

All terms in this equation will be of the same order of magnitude if we choose the following quantities to be constants, independent of time: (i) the velocity of the pinch point a_t; (ii) the leading-order pressures in these regions, $P - 3!A_{\pm}$; and (iii) the time derivative of the length scale squared. To express this constancy we use the notation

$$a_t = u , \tag{60}$$

$$L^{\pm}_t L^{\pm} = -3A_{\pm} , \tag{61}$$

with u being independent of time. Note then that the solution for a and L is

$$a = u\epsilon , \tag{62}$$

$$L^{\pm} = \sqrt{6A_{\pm}\epsilon} . \tag{63}$$

Thus, the lowest-order result, Eq. (59), becomes

$$\partial^4_{\mu}F_{\pm} - (4 - \mu\partial_{\mu})F_{\pm}/\mu^2 = u . \tag{64}$$

Since Eq. (64) is linear we can analyze its solutions rather fully. Notice that it is a fourth-order inhomogeneous ordinary differential equation, with irregular singular points at infinity and zero [8]. One solution to the inhomogeneous equation is simply $u\mu^4/4!$. A more general but equally simple solution involves one undetermined constant of integration, and is

$$F^0_{\pm}(\mu) = u\mu^4/4! + \gamma_{\pm}F_2(\mu) . \tag{65}$$

Here, $\gamma_{\pm}$ are constants of integration, yet to be determined, and F_2 is the simple solution to the homogeneous equation

$$F_\mu(\mu)=\mu^2+2\mu^4/4!=\mu^2 f_2(\mu^2)\ . \tag{66}$$

The subscript 2 is intended as a reminder that the lowest power of μ in this expression is μ^2. The f_2 notation will be convenient when we discuss the other three solutions. Later we shall discuss the additional more complex solutions to the homogeneous equation which start off with third, first, and zeroth powers of μ. However for now, we should see what we can do to fit the solution expressed in Eqs. (65) and (66) onto Eq. (53), which expresses the form of g in the pinch region. Use Eqs. (55), (60), and (61) to reexpress

$$g(x,t)\sim A_\pm y^3+(u+2\gamma_\pm)y^4/4!+\gamma_\pm (L^\pm)^2 y^2\ . \tag{67}$$

The first terms on the right-hand side of Eq. (67) each have direct analogs in Eq. (53), so we cannot learn very much from them. However, the last term in Eq. (67) is quite interesting. It should be compared with the corresponding term in Eq. (53),

$$-Jy^2\log_{10}(|y|/J)/6A_\pm\ .$$

Analyze this term for μ of order unity, where to logarithmic accuracy it is

$$-Jy^2\log_{10}(L^\pm/J)/6A_\pm\ .$$

If we say that there should be an order-of-magnitude equality between these two y^2 terms and postpone the question of whether a full match can be achieved, then we should argue that

$$J\log_{10}(L^\pm/J)\sim\gamma_\pm(L^\pm)^2\sim\epsilon\sim(t_e-t)$$

so that

$$J\sim\epsilon\log_{10}\epsilon^{-1}\ . \tag{68}$$

The logarithm in Eq. (68) is a correct estimate of the order of $\log_{10}(|y|/J)$ when y is of order $L^\pm$. Now we have to see to what extent we can make the analysis stand up to a more full treatment.

3. *Intermediate regions II*

We now try to construct a more careful analysis. Return to the solutions of the homogeneous form of Eq. (64). This is a fourth-order equation. We have one solution. Assume that these are expressed as an asymptotic expansion about $y=0$, with lead terms of order μ^p, with p being 3, 1, and 0. Expressed as expansions in powers of μ, these solutions are

$$F_3(\mu)=\mu^3 f_3(\mu^2)\ , \tag{69}$$

$$F_1(\mu)=\mu f_1(\mu^2)+\mu^3\log_{10}(|\mu|)f_3(\mu^2)\ , \tag{70}$$

$$F_0(\mu)=f_0(\mu^2)-\mu^2\log_{10}(|\mu|)f_2(\mu^2)\ . \tag{71}$$

Our notation with the f's is helpful because in each case the f has a power-series expansion in its argument, starting with a constant term. It is easy to see that these f's are entire functions of their arguments. Note the logarithms in Eqs. (70) and (71). These logarithms will be used to match corresponding logarithms in Eq. (53). The general solution to Eq. (64) is the sum of the solution (64) plus arbitrary coefficients, which may differ in the two regions, times the terms in Eqs. (69)–(71). However, these solutions can show exponential blowup as μ goes to $\pm\infty$. To see this property, write

$$F_j(\mu)=\exp[X_j(\mu)]\ ,$$

and assume that X_j goes to infinity at the appropriate infinity for μ. Then, Eq. (64) implies that X_j (abbreviated as just X) obeys, in the asymptotic limit

$$(X_\mu)^3=-\frac{1}{\mu}\ ,$$

so that for large $|\mu|$

$$X=-\tfrac{3}{2}e^{2\pi p/3}|\mu|^{2/3}\ , \tag{72}$$

where $p=0$ or 1 or -1. The general solution to the inhomogeneous equation is then of the form of the sum of Eq. (64) (which contains the constant of integration $\gamma_\pm$) and a sum of three terms which are obtained as linear combinations of the solutions Eqs. (65) and (66) and are, respectively, proportional to

$$\exp\{-\tfrac{3}{2}|\mu|^{2/3}\}\ ,$$

$$\exp\{\tfrac{3}{4}(1-\sqrt{3}\iota)|\mu|^{2/3}\}\ ,$$

$$\exp\{\tfrac{3}{4}(1+\sqrt{3}\iota)|\mu|^{2/3}\}\ .$$

At first sight, one might argue that the exponential blowup of the latter two terms means that their coefficients should be zero, while the decay of the first of these three means that it would not contribute for large values of $|\mu|$. However, when μ gets large the solutions $F_\pm$ get large and thus the expansion of Eq. (57) breaks down. Hence, we can only employ this analysis when $|\mu|$ is not too large, say of order $\log_{10}L$ or smaller. In this region it is just fine to use all four terms in the expansion and write

$$\begin{aligned} g(y)&=A_\pm y^3+F_\pm(\mu)L_\pm^4\\ &=A_\pm y^3+L_\pm^4\{u\mu/4!+\gamma_\pm F_2(\mu)+\alpha_\pm F_0(\mu)\\ &\qquad+\beta_\pm F_1(\mu)+\bar\omega_\pm F_3(\mu)\}\ . \end{aligned} \tag{73}$$

To match onto the pinch region, take the small μ form of each of the F's. The result is

$$\begin{aligned} g(y)=&(A_\pm+\bar\omega_\pm L^\pm)y^3+F_\pm(\mu)L_\pm^4+(u+2\bar\omega_\pm)y^4/4!+\bar w_\pm y^2(L^\pm)^2\\ &+\alpha_\pm\{(L^\pm)^4+2(L^\pm)^2y^2\log_{10}(y/L^\pm)+y^4\log_{10}(y/L^\pm)/6\}+\beta_\pm(L^\pm)^3y(1+\mu^2)\ . \end{aligned} \tag{74}$$

When we fit this to the outer solution of Eq. (53), we need as many arbitrary coefficients as we can get, each of which does not go to zero as t goes to t_c. However, there is nothing in Eq. (53) which corresponds to the β term in Eq. (74), so that coefficient is set equal to zero. The remaining terms all fit onto the pinch region when we make the correct choices of the fitting coefficients. The only unexpected feature is that we cannot choose $\alpha_{\pm}$ to be of order unity. Instead we must choose this coefficient to be small (but only logarithmically so)

$$\alpha_{\pm} \sim [\log_{10}(\epsilon^{-1})]^{-1} . \tag{75}$$

With this choice, the terms in y^2, $y^2\log_{10}(y)$, y^4, and $y^4\log_{10}(y)$ all work out perfectly. The $\overline{\omega}_{\pm}L^{\pm}$ is absorbed into a redefinition of $A_{\pm}$. The constant term $\alpha_{\pm}(L^{\pm})^4$ is just right to fit a K for which

$$K_t \sim J \sim \epsilon/\log_{10}(\epsilon^{-1}) ,$$

so that

$$K \sim \epsilon^2/\log_{10}(\epsilon^{-1}) \sim \alpha_{\pm}(L^{\pm})^4 . \tag{76}$$

We have already seen that these estimations agree well with the simulations.

V. CONCLUSIONS

In this paper we have studied the droplet-breakup problem in the Hele-Shaw cell. Lubrication approximations are used to derive equations for the width of a thin neck between two masses of the fluid. These equations can be used to describe the singularity-development process. Starting from smooth initial flows which are different from those in previous studies [9–12] we have observed finite-time singularity in the solutions of these partial differential equations. For $\rho \neq 0$ or the inertial case, when $t \rightarrow t_c$, we have observed terms with power-law behaviors which are explained by a simple scaling argument. For $\rho = 0$ or the no-inertia case, and for the case where we have finite-time singularity, when t is very close to the critical time t_c, matched asymptotic similarity solutions are found for the shape of the interface in the pinch region and the intermediate region. Comparison between the simulation results and theoretical universal shapes are made and the agreements are very satisfying.

ACKNOWLEDGMENTS

The authors express their appreciation to the many people who have discussed this work with them, many of whom made remarks which significantly influenced our work. We particularly want to mention the following people: Andrea Bertozzi, Michael Brenner, Sidney Nagel, and Henry Rachford. During the course of this work we received support from The University of Chicago Materials Research Laboratory and The U.S. Department of Energy.

[1] P. Constantin, T. F. Dupont, R. E. Goldstein, L. P. Kadanoff, M. Shelley, and S.-M. Zhou, preceding paper, Phys. Rev. E **47**, 4169 (1993).
[2] H. S. S. Hele-Shaw, Nature **58**, 34 (1898).
[3] Note that certain experiments reported in Ref. [4] involving two viscous fluids, rather than air and water, exhibit behavior qualitatively different from those described here.
[4] R. E. Goldstein, T. G. Mason, and E. Shyamsunder (private communication).
[5] M. J. Shelley, R. E. Goldstein, and A. I. Pesci (unpublished).
[6] A. Cameron, *Principles of Lubrication* (Longmans, London, 1966).
[7] C. Bender and S. Orszag, *Advanced Mathematical Methods for Scientists and Engineers* (McGraw-Hill, New York, 1978).
[8] E. A. Coddington and N. Levinson, *Theory of Ordinary Differential Equations* (McGraw-Hill, New York, 1955).
[9] *Dynamics of Curved Fronts,* edited by P. Pelce (Academic, San Diego, 1988), and references therein.
[10] E. Meiberg and G. M. Homsy, Phys. Fluids **31**, 429 (1988).
[11] G. Tryggvason and H. Aref, J. Fluid Mech. **136**, 1 (1983); **154**, 287 (1985).
[12] A. J. Degregoria and L. W. Schwartz, Phys. Rev. Lett. **58**, 1742 (1987).